SUPPLEMENTARY INFORMATION

Signature of transition to supershear rupture speed in coseismic off-fault damage zone

Jorge Jara[1,*], Lucile Bruhat[1], Marion Y. Thomas[2], Solène Antoine[3], Kurama Okubo[4], Esteban Rougier[5], Ares J. Rosakis[6], Charles G. Sammis[7], Yann Klinger[3], Romain Jolivet[1,8] and Harsha S. Bhat[1]

1. Laboratoire de Géologie, Département de Géosciences, École Normale Supérieure, CNRS, UMR 8538, PSL Université, Paris, France
2. Institut des Sciences de la Terre de Paris, Sorbonne Université, CNRS, UMR 7193, Paris, France
3. Université de Paris, Institut de Physique du Globe de Paris, CNRS, 75005 Paris, France
4. National Research Institute for Earth Science and Disaster Resilience, 3-1 Tennnodai, Tsukuba 305-0006, Ibaraki, Japan
5. EES-17 – Earth and Environmental Sciences Division, Los Alamos National Laboratory, Los Alamos, NM, USA
6. Graduate Aerospace Laboratories, California Institute of Technology, Pasadena, California, 91125, USA
7. Department of Earth Sciences, University of Southern California, Los Angeles, CA 90089, USA
8. Institut Universitaire de France, 1 rue Descartes, 75005 Paris, France

* Corresponding Author: jara@geologie.ens.fr

Last Modified on Mon 3rd May, 2021 at 15:41:30

S1. Numerical modeling of off-fault coseismic damage

Specific parameters used in the FDEM model are provided in table S1 and those used in the micromechanics based model are provided in table S2.

Table S1: Parameters for contact interactions within the off-fault medium, FDEM model.

Parameters	Description	Values
G_{IC}	Fracture energy for tensile cohesion (kJ/m^2)	3.0
C_I	Cohesion for mode I opening crack (MPa)	8.0
$\delta_{c,I}$	Critical cohesive weakening displacement in tension (mm)	0.75
G_{IIC}	Fracture energy for shear cohesion (kJ/m^2)	20.0
C_{II}	Cohesion for mode II shear crack (MPa)	27.5
$\delta_{c,II}$	Critical cohesive weakening displacement in shear (mm)	1.5
$f_{s,o}$	Static friction coefficient	0.6
$f_{d,o}$	Dynamic friction coefficient	0.1
G^f_{IIC}	Shear fracture energy for friction (kJ/m^2)	20.0
δ^f_{II}	Critical weakening displacement for friction (mm)	1.67

Table S2: Parameters used for the micromechanical model

Parameters	Description	Values
a_0	Penny shape crack radius (m)	60
N_v	Volume density of cracks ($\times 10^{-7}$ #/m^3)	1.68
D_0	Initial damage density	0.1
v_m	branching speed (km/s)	1.58
β	*Ashby and Sammis* (1990) factor	0.1
Ω	Crack factor	2.0
t^*	*Prakash and Clifton* (1993) time (s)	40×10^{-3}

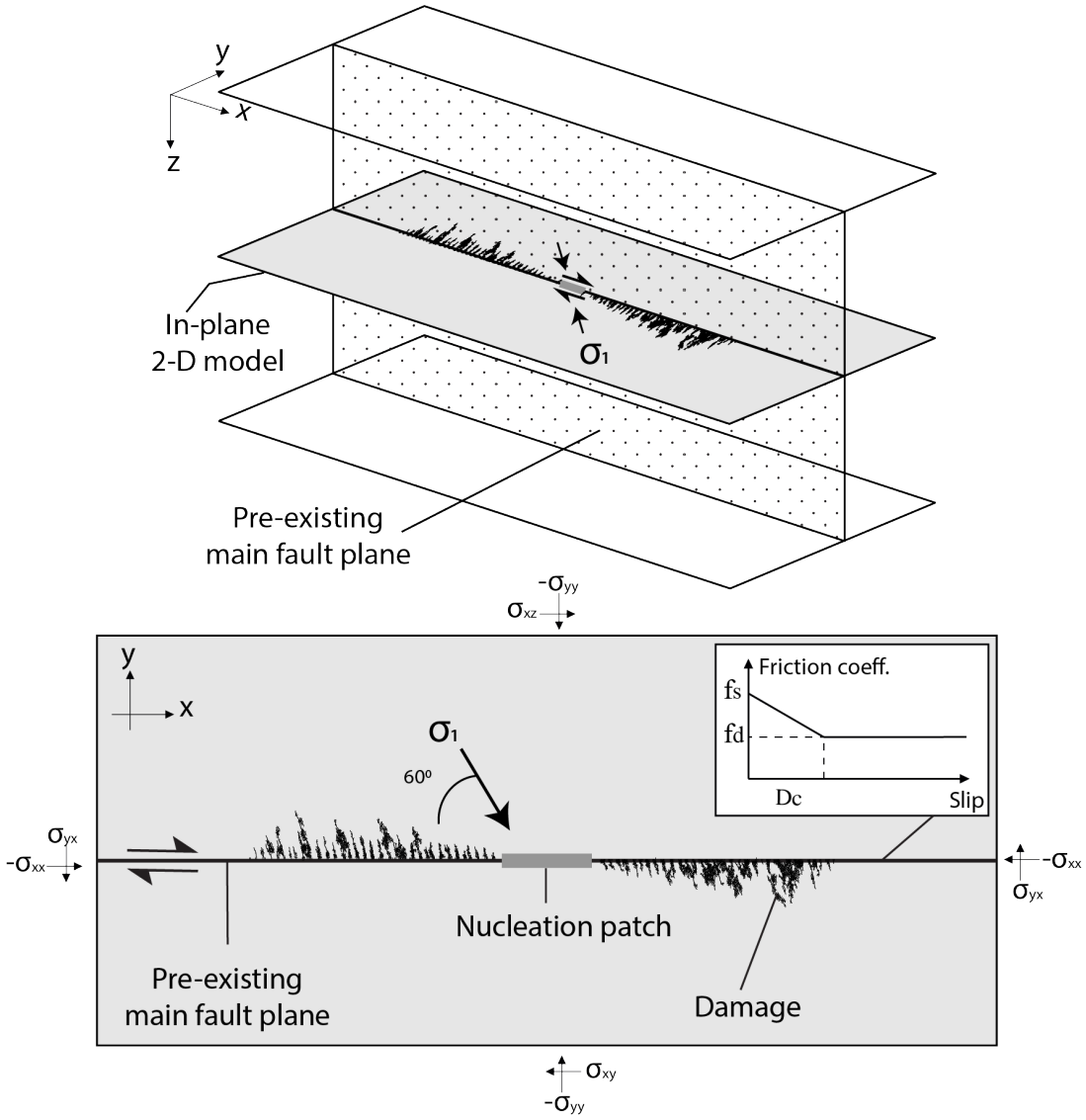

Figure S1: Schematics and parameters used for the simulations of dynamic ruptures in a 2-D in-plane model. We consider a right-lateral planar fault, embedded in a brittle off-fault medium (FDEM or micromechanical model). Slip-weakening friction (grey box) acts along the main fault plane.The medium is loaded by uniform background stresses with the maximum compressive stress σ_1 making an angle of 60^o with the fault plane. The thick grey line corresponds to the nucleation zone where either the initial shear stress is set-up to be just above the fault strength (micromechanical model), or we apply a local decrease of the static friction (FDEM model). Figures adapted from *Thomas et al.* (2017) and *Okubo et al.* (2019)

.

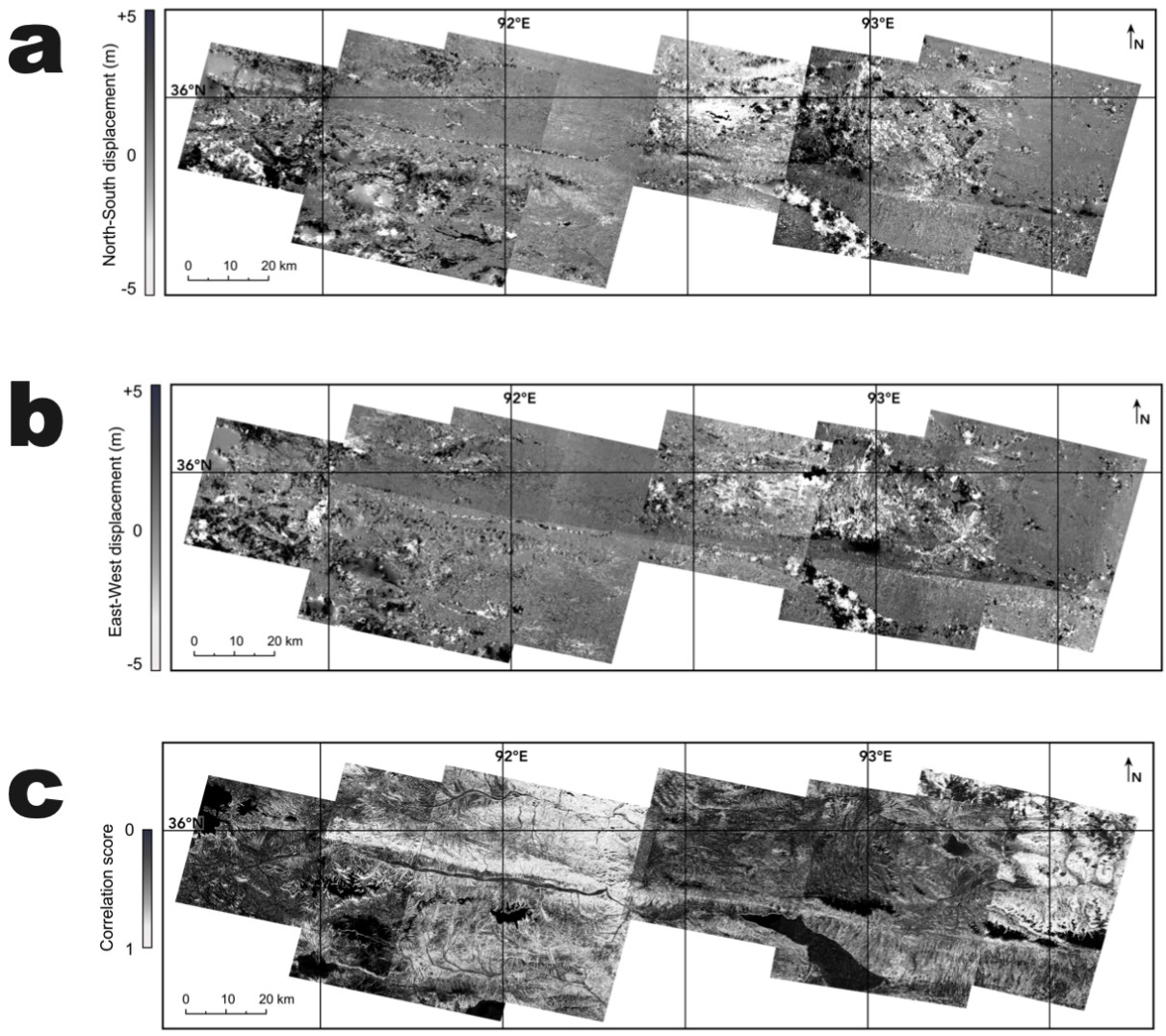

Figure S2: (a) North-South and (b) East-West surface displacement maps for the strike-slip part of the 2001 Kunlun surface rupture. Results benefit from a 10-meters ground resolution after the horizontal correlation of SPOT (1 to 4) pre- and post-earthquake images using MicMac. North-South displacements are close to zero at the fault while there is a clear left-lateral offset in the East-West displacement map. (c) Correlation score provided by MicMac after the horizontal correlation of the SPOT images. Dark areas correspond to decorrelation in lakes, drainages or snow. White areas, representing areas of good correlation, are present around the fault zone and particularly between 91.5 and 92.5^o E.

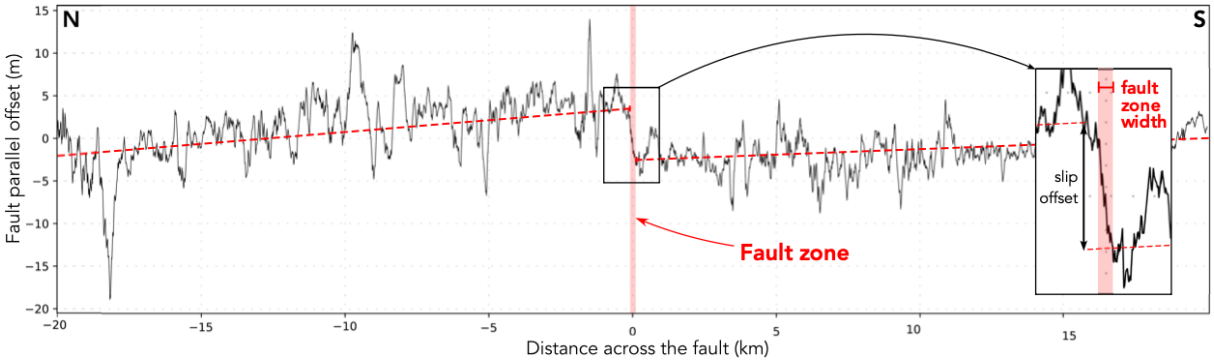

Figure S3: Example of one of the 396 profiles obtained from the optical correlation image processing along the fault. The step in the figure represents the coseismic offset produced by the earthquake, while the red box denotes the region defined during this work as the width of the off-fault damage zone.

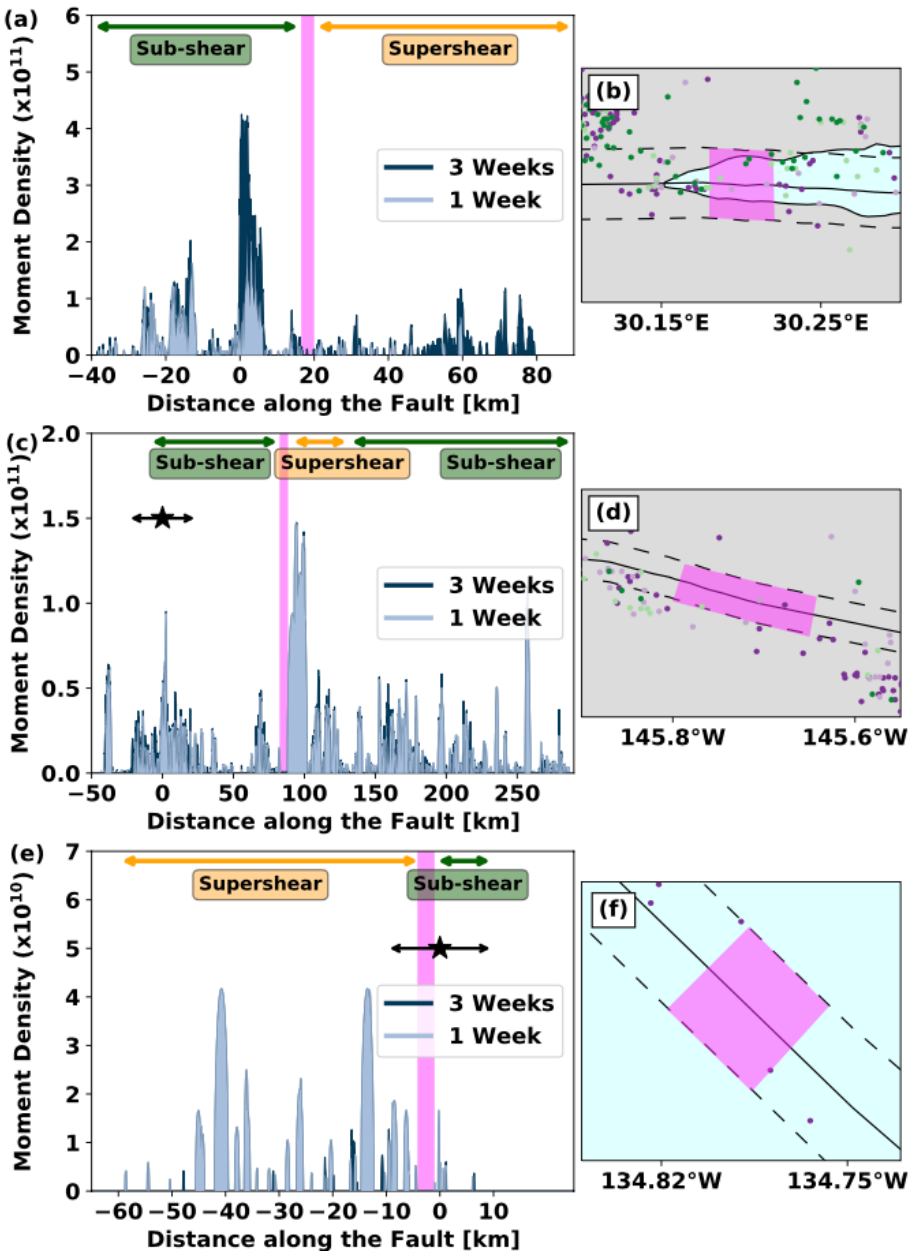

Figure S4: Spatio-Temporal Seismic Moment Density Evolution. Cumulative aftershock seismic moment density projected on the main fault at different temporal scales (1-3 weeks), for Izmit (**a**), Denali (**c**), and Craig (**e**) earthquakes. All the aftershocks within a distance of 2.5 km from the fault are considered in the calculation (area denoted by the black discontinuous lines in Figures **6a**, **b** and **c** on the main text). Color-coded arrows (on top of **a**, **b**, and **c**) indicate the different speed regimes reported for each event (green for sub-Rayleigh and orange for supershear) (*Bouchon and Karabulut*, 2008, *Ellsworth et al.*, 2004, *Yue et al.*, 2013), while the starts denote the epicenter of each earthquake and the arrows indicate the ruptures' direction. The pink boxes point out our proposed transition zone, also observed in a map view in **b** for Izmit, **d** for Denali, and **f** for Craig earthquakes.

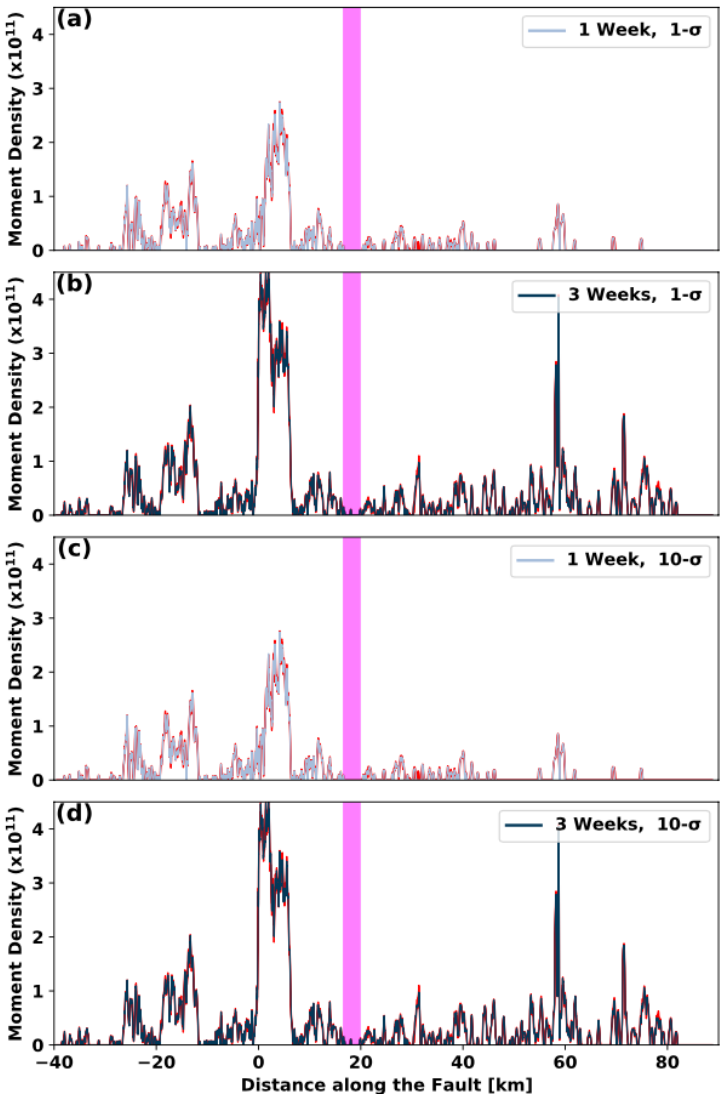

Figure S5: High-Resolution Aftershock Catalog Statistical Analysis, Izmit Earthquake, 1-and 10-σ. **a** and b show the aftershock seismic moment density projected on the main fault at different temporal scales (1-3 weeks), considering all the aftershocks at a distance of 5 km from the fault. The red area in each panel denotes the mean seismic moment density projected on the main fault $\pm$ the standard deviation (1-σ, indicated in the legend) of the 10000 synthetics catalogs performed for the analysis. The pink box indicates this work's proposed transition zone. **c** and **d** are the same plots than before (**a** and **b**), but considering a 10-σ standard deviation on the calculation.

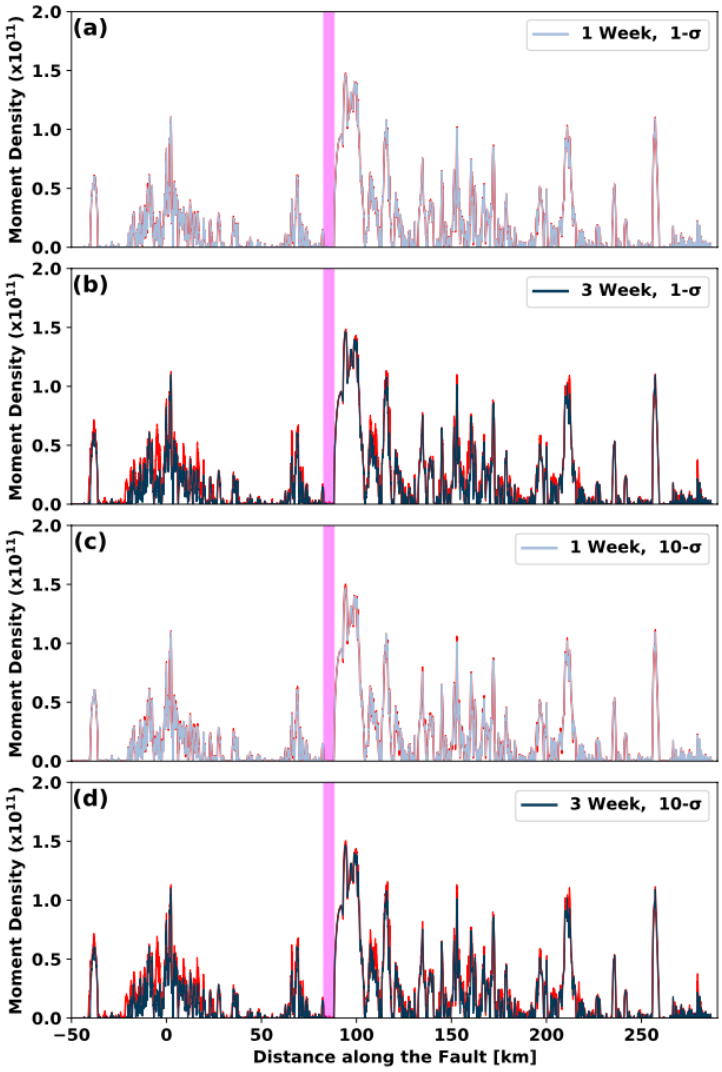

Figure S6: High-Resolution Aftershock Catalog Statistical Analysis, Denali Earthquake, 1-and 10-σ. **a** and b show the aftershock seismic moment density projected on the main fault at different temporal scales (1-3 weeks), considering all the aftershocks at a distance of 5 km from the fault. The red area in each panel denotes the mean seismic moment density projected on the main fault $\pm$ the standard deviation (1-σ, indicated in the legend) of the 10000 synthetics catalogs performed for the analysis. The pink box indicates this work's proposed transition zone. **c** and **d** are the same plots than before (**a** and **b**), but considering a 10-σ standard deviation on the calculation.

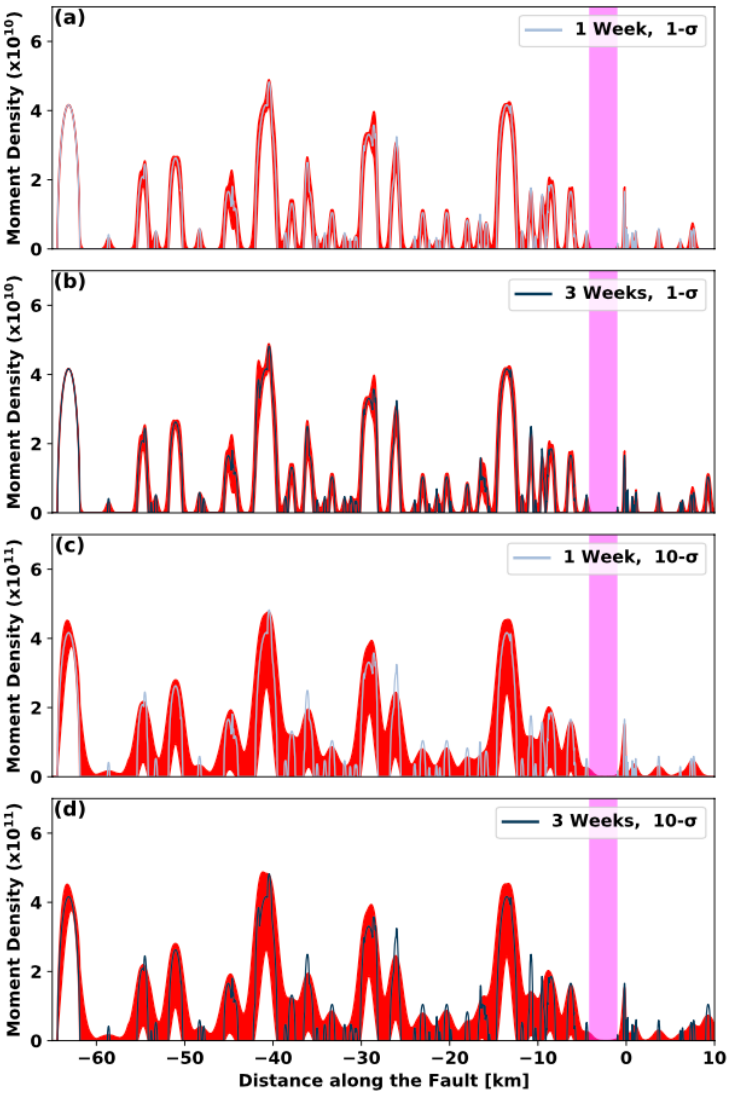

Figure S7: High-Resolution Aftershock Catalog Statistical Analysis, Craig Earthquake, 1-and 10-σ. **a** and b show the aftershock seismic moment density projected on the main fault at different temporal scales (1-3 weeks), considering all the aftershocks at a distance of 5 km from the fault. The red area in each panel denotes the mean seismic moment density projected on the main fault $\pm$ the standard deviation (1-σ, indicated in the legend) of the 10000 synthetics catalogs performed for the analysis. The pink box indicates this work's proposed transition zone. **c** and **d** are the same plots than before (**a** and **b**), but considering a 10-σ standard deviation on the calculation.

References

Ashby, M. F., and C. G. Sammis, The damage mechanics of brittle solids in compression, *Pure and Applied Geophysics PAGEOPH*, *133*, 489–521, 1990.

Bouchon, M., and H. Karabulut, The Aftershock Signature of Supershear Earthquakes, *Science*, *320*, 1323–1325, 2008.

Ellsworth, W. L., et al., Near-Field Ground Motion of the 2002 Denali Fault, Alaska, Earthquake Recorded at Pump Station 10, *Earthquake Spectra*, *20*, 597–615, 2004.

Okubo, K., H. S. Bhat, E. Rougier, S. Marty, A. Schubnel, Z. Lei, E. E. Knight, and Y. Klinger, Dynamics, Radiation, and Overall Energy Budget of Earthquake Rupture With Coseismic Off-Fault Damage, *Journal of Geophysical Research: Solid Earth*, *124*, 11,771–11,801, 2019.

Prakash, V., and R. J. Clifton, Time resolved dynamic friction measurements in pressure shear, in *American Society of Mechanical Engineers, Applied Mechanics Division, AMD*, American Society of Mechanical Engineers, 1993.

Thomas, M. Y., H. S. Bhat, and Y. Klinger, Effect of Brittle Off-Fault Damage on Earthquake Rupture Dynamics, in *Fault Zone Dynamic Processes: Evolution of Fault Properties During Seismic Rupture*, pp. 255–280, AGU AMERICAN GEOPHYSICAL UNION, 2017.

Yue, H., T. Lay, J. T. Freymueller, K. Ding, L. Rivera, N. A. Ruppert, and K. D. Koper, Supershear rupture of the 5 January 2013 Craig, Alaska (M w 7.5) earthquake, *Journal of Geophysical Research: Solid Earth*, *118*, 5903–5919, 2013.